Molecular Dynamics Simulation of Trimer Self-Assembly Under Shear[☆]

Raymond D. Mountain[a], Harold W. Hatch[a], Vincent K. Shen[a]

[a] *Chemical Informatics Research Group, Chemical Sciences Division, National Institute of Standards and Technology, Gaithersburg, Maryland 20899-8380, USA*

Abstract

The self-assembly of patchy trimer particles consisting of one attractive site and two repulsive sites is investigated with nonequilibrium molecular dynamics simulations in the presence of a velocity gradient, as would be produced by the application of a shear stress on the system. As shear is increased, globular-shaped micellar clusters increase in size and become more elongated. The globular clusters are also more stable at higher temperatures in the presence of shear than at equilibrium. These results help to increase our understanding of the effect of shear on self-assembly for a variety of applications.

Keywords: self-assembly, colloids, shear, computer simulation

1. Introduction

While self-assembly is a promising route to fabricate new materials, practical length scales for fabrication are limited by the formation of defects [1]. In order to exploit self-assembly in technological applications, self-assembly may be directed by external fields, templates or specific chemical interactions in order to promote long-range ordering [2]. One example of directed self-assembly is the application of shear to block copolymer thin films, which has been shown to reduce defects and impose long-range order and alignment of the self-assembled structures as templates for nanolithography [3]. In addition, studies of *de novo* materials design of bioinspired silk fibers find that shear enhances alignment of polymers to improve the mechanical properties of the material [4, 5]. Shear may also play a role in extrusion of self-assembled materials for industrial applications [6, 7]. Self-assembly under shear has been the subject of many experimental, theoretical and computational studies. Experimental studies of shear-induced self-assembly include block copolymer thin films [8, 3, 9, 10, 11, 12], worm-like micelles [13, 14], carbon nanotubes [15] and colloidal crystals [16, 17]. Theoretical and particle-based simulations are useful because they elucidate the mecha-

[☆]Contribution of the National Institute of Standards and Technology, not subject to U.S. Copyright.

nism of self-assembly under shear in block copolymers [18, 19, 20, 21, 22, 23, 24] and micelles [25, 26]. Studies of aggregation under shear also provide insight into the ability of shear to enhance and hinder cluster formation [27, 28].

While many of the previous studies of self-assembly under shear involved molecular systems, colloids with anisotropic shapes and interactions under shear are less well understood. Recent advances in colloidal synthesis have led to the creation of a variety of patchy colloids including rods, lock and key colloids, cubic colloids and colloidal clusters [29, 30]. Nikoubashman *et al.* simulated the self-assembly of Janus particles under shear, and found that moderate shear enhances the aggregation of spherical clusters [31, 32]. In addition, DeLaCruz-Araujo *et al.* simulated the aggregation of Janus particles under shear into micelles, wormlike clusters, vesicles and lamellae *via* Brownian dynamics [33]. In this work, we apply shear to trimers consisting of one attractive site and two repulsive sites. The trimers in this work are qualitatively similar to the recently synthesized patchy colloidal trimers consisting of one smooth and two rough beads, where the smooth beads possess an attractive interaction in the presence of depletant molecules in solution [34]. While these trimers have been the subject of thermodynamic studies [34, 35, 36, 37], there have been no studies on the dynamics of these particles. In addition, the trimer particles geometrically resemble the Y-shape of monoclonal antibodies, and the study of these particles under shear may aid in understanding aggregation-driven increases in the viscosity of monoclonal antibody solutions, with an application of improving the delivery of biological pharmaceuticals [38, 39]. Although the model in this work is not as short ranged as the protein and colloid systems described above, the model may be used to capture basic aspects of real systems.

In this work, molecular dynamics simulations of trimers consisting of one attractive site and two repulsive sites are performed in the presence of a velocity gradient, as would be produced by the application of shear stress. These trimers were shown previously [35] to self-assemble into globular-shaped clusters at equilibrium. We find that increasing the shear stabilizes larger clusters, and shear also leads to an increase in tubular structures.

This paper is organized as follows. In Section 2, the model for the trimer particles studied in this work is presented. The nonequilibrium molecular dynamics simulations are described in Section 3. In Section 4, the distribution of cluster sizes, the short range spatial order of the trimers in a cluster, and the potential energy of the system are examined. Finally, conclusions are provided in Section 5.

2. Model

The system consists of 500 rigid trimers. Each trimer is composed of an attractive site and two repulsive sites located at a distance L from the attractive site with bond angles of 60°, as shown in Fig. 1 and described in Ref. [35]. The attractive sites interact via a Lennard-Jones potential $\phi(r)$,

$$\phi(r) = 4\epsilon[(\sigma/r)^{12} - (\sigma/r)^{6}]. \quad (1)$$

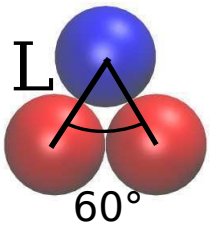

Figure 1: The trimer model investigated in this work is illustrated using the Visual Molecular Dynamics program [43]. The blue site is attracted to other blue sites. All other pair interactions are purely repulsive.

The Lennard-Jones interaction is truncated at $r = 3\sigma$ in the shifted-force form [35]. The interaction between all other site pairs is through a repulsive interaction $\psi(r)$ of the Weeks-Chandler-Anderson form [40]

$$\psi(r) = \begin{cases} \phi(r) + \epsilon & : r < 2^{1/6}\sigma \\ 0 & : r \geq 2^{1/6}\sigma. \end{cases} \tag{2}$$

Each of the particles in a trimer has mass m. The units of mass, length and energy used in the simulation have unit values so that $m = 1$, $\sigma = 1$ and $\epsilon = 1$ with the result that the time unit $\tau = \sqrt{\epsilon/m\sigma^2} = 1$ as well. The bond length L is set to 1 in these simulations. Unless noted otherwise, reduced units are reported. Note that the solvent is modeled via the effective interaction between the particles. Thus, the effective interaction amounts to a potential of mean force, as could be obtained by integrating over the solvent degrees of freedom. Accordingly, the model simulated here lacks explicit solvent and ignores some solvent mediated phenomena, such as hydrodynamic effects and buffeting due to random forces. Although hydrodynamics can influence dynamical properties in non-equilibrium self-assembly processes [41], implicit solvent simulations allow for the simulation of larger system sizes [42] and have been shown to possess similar self-assembled structural properties as explicit solvent simulations [41].

3. Methods

The system of 500 trimers was placed in a rigid cubic cell with cell edge of 23.2 units so that the number density of the system was 0.04, or 6% packing fraction (see Figure 2 for a visualization of this density). Periodic boundary conditions were applied in all three dimensions. The equations of motion were integrated using a Velocity-Verlet algorithm [44] modified [45] so that the orientation of the trimers was described using quaternions [46]. The time step for integration of the equations of motion was $\delta t = 0.01\tau$ for all cases unless otherwise indicated. This time step is sufficiently small, because it is expected to lead to a root-mean-squared fluctuation in energy approximately on the order of magnitude of 10^{-3} [47]. Simulations were performed in the canonical ensemble. The temperature of the system was maintained using separate Nóse-Hoover

thermostats [44] for the translational and orientational degrees of freedom. The thermostats had a response time of 1 τ as this provides good control of the temperature of the system.

In order to examine the influence of shear on the cluster formation, a velocity gradient was established using the Reversed Perturbation Nonequilibrium molecular dynamics method [48, 49, 50]. A set of 16 layers was established normal to the z-direction of the simulation cell. At a specified time interval the momentum of the particle with the largest positive x-component of momentum in the first layer was exchanged with the momentum of the particle in the ninth layer with the largest negative x-component of momentum. This results in a gradient of the x-component of momentum in the z-direction while conserving the energy of the system. For the cases considered here, three values of the exchange interval were used, specifically 1.1 τ for the small gradient, 0.7 τ for the intermediate velocity gradient, and 0.3 τ for the large gradient case. Note that care must be taken for constant temperature simulations with Reversed Perturbation Nonequilibrium molecular dynamics method [48, 49]. In particular, the thermostat response time was chosen to be slow enough such that it did not influence the velocity profile, and the exchange interval was chosen to be long enough such that a large temperature profile did not develop across the simulation cell.

Simulations were first prepared at a high temperature of $T = 0.5$, where the fluid was homogeneous. The velocity gradient was then imposed over a duration of 1000 τ using one of the momentum swap rates noted above. After this period, once the velocity profile became linear, the temperature was reduced using the procedure described below to the desired temperature of 0.4, 0.375, 0.35, 0.325, 0.3, 0.275, 0.25, 0.225 or 0.2 while maintaining the same momentum swap rate in order to maintain a linear velocity gradient.

The procedure used to change the temperature of the system was the same in all cases. First the specified temperature set by the thermostats was changed and the system was run for 10^3 time steps with $\delta t = 10^{-4}$ τ. Then the time step was increased to 10^{-2} τ and run for 1000 τ. At this point, the temperature stabilized, but the potential energy of the system was not stabilized. As will be shown, the potential energy requires some additional time before it assumes a stable value.

As the system evolves from a liquid-like configuration at $T = 0.5$ to a heterogeneous set of clusters for $T \leq 0.3$, the potential energy of the system decreases. Clusters were defined as all trimers having an attractive site within a cut-off distance, 1.3, from at least one other attractive site in the cluster (see Appendix A) [51]. Only when the distribution of cluster sizes has stabilized does the potential energy achieve a stable, time-independent average value with fluctuations about the mean value. The fluctuations in the potential energy were a consequence of the variation in time of the distribution of cluster sizes.

The potential energy was monitored by constructing block averages of 10 τ duration that were recorded for later processing. The "length" and the number of clusters containing N_C trimers, as described in Appendix A, was determined at 10 τ intervals. The averages of these quantities were recorded at 200 τ

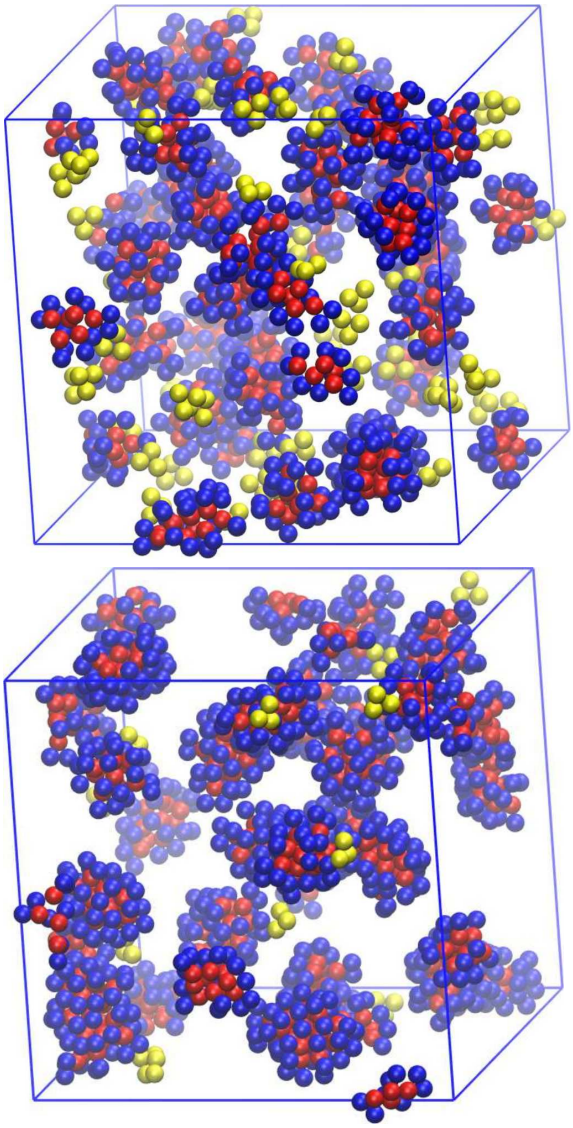

Figure 2: The system of trimers as described in Section 3 with $T = 0.25$ and the periodic cell shown by the blue square for (top) no shear and (bottom) the highest exchange rate investigated (*i.e.*, high shear). Particles shown in yellow are in clusters of three or less other particles (see Appendix A for cluster definition). Otherwise, particles in clusters of size four or greater are colored red and blue. There are noticeably less yellow particles in the shear case than in the no shear case. Although shear was applied in the horizontal direction, the clusters have no apparent visual correlation with this shear direction.

intervals.

In order to obtain a stable value for the potential energy, and therefore for the cluster size distribution, simulations of at least 20 000 τ following the quench into the cluster forming region were needed. The results of this process are labeled "stabilized configurations". The results discussed here are determined from simulations of 20 000 τ up to 80 000 τ duration that start from a stabilized configuration with a velocity gradient. The required length of the simulation was based on the stability of the block averaged energies.

4. Results and Discussion

The objective of this study was to determine how the presence of a velocity gradient, as would be developed by the application of shear to the fluid, modifies the stability of clusters in the model system. Using the Reversed Perturbation Nonequilibrium molecular dynamics method [48, 49], a momentum flux was imposed on the system which resulted in a velocity gradient. The shear rate was then obtained as the slope of the resulting velocity gradient, and the viscosity was obtained from this shear rate and the momentum flux, shown in Figure 3. For all temperatures investigated, the fluid has a slight tendency to thicken as the shear rate increases, but the standard error in the reported viscosity is the same order of magnitude as the change in viscosity. The possibility that the viscosity is independent of shear rate (*i.e.* Newtonian) is shown by the linear fits in Figure 3, where all of the data fall within 2 standard error of the fits. In any case, the fluid is either Newtonian, or possesses a slight tendency to shear thicken. This is consistent with the lower shear rate regimes observed in some experiments for micellar systems [52, 53].

An illustration of the system with no shear and the highest shear investigated is shown in Figure 2. Clusters appear to be stabilized by the presence of a velocity gradient under these conditions. There are three quantitative indicators that we used to examine the effects of temperature on the steady state properties of clusters in a system with a velocity gradient. These are the average potential energy per trimer, the pair distribution of the attractive sites, and the distribution of the mass of the system in clusters as a function of the number of trimers in a cluster.

The potential energy per trimer decreases with decreasing temperature from $T = 0.5$ with the steepest change around $T = 0.3$, the region of the transition from a fluid-like structure to the presence of clusters plus void regions. This corresponds to a maximum in the heat capacity near $T = 0.3$. For a given temperature, the potential energy decreases as the velocity gradient increases. This is indicated in Fig. 4 for each of the states examined. The resulting specific heat was larger for larger values of the velocity gradient as the temperature decreases from 0.5 to 0.3. The limited temperature spacing of the states precludes precise determination of the magnitude and location of the maximum in the specific heat indicated in the insert in Fig. 4.

The pair distribution function for the attractive sites of the trimers has a single maximum for $T = 0.5$ for near neighbor distances and is flat for larger

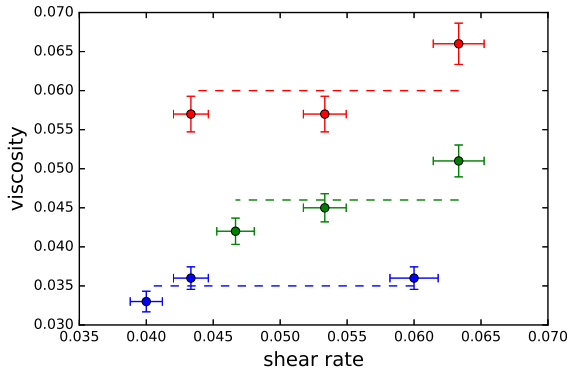

Figure 3: The reduced viscosity as a function of shear rate for the following temperatures: (blue) $T = 0.2$, (green) $T = 0.3$ and (red) $T = 0.4$. The dashed lines are linear fits with zero slope, to serve as a guide to the eye. The standard error is shown by the error bars.

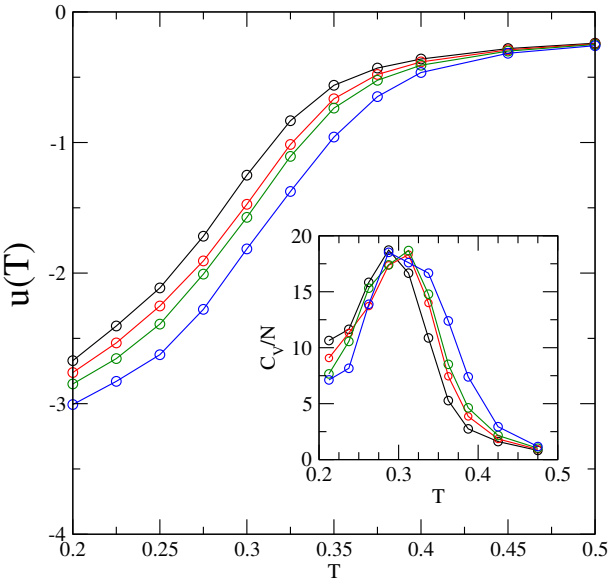

Figure 4: The average potential energy per trimer, u, as a function of temperature, T, for the case of no velocity gradient (black), small velocity gradient (red), medium gradient (green) and large gradient (blue). The lines are a guide for the eye. The standard deviation of the potential energy is smaller than the symbols. The insert displays the heat capacity.

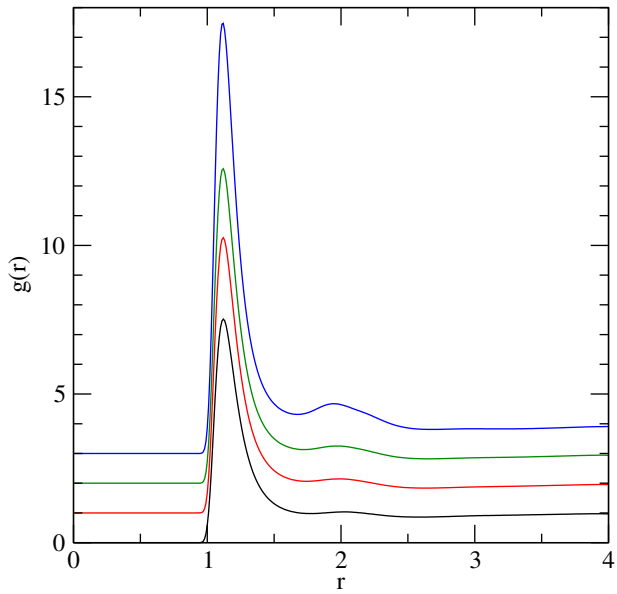

Figure 5: The radial distribution functions, $g(r)$ at $T = 0.35$ for the attractive site pairs are shown for the case of no velocity gradient (black), small velocity gradient (red), medium gradient (green) and large gradient (blue). The functions are vertically offset for clarity.

separations. This structure persisted as the temperature was lowered until to about $T = 0.35$ for the case with the large velocity gradient when a weak secondary maximum corresponding to the second neighbors appears as shown in Fig. 5. This feature develops for other cases when $T = 0.3$, as shown in Fig. 6. Additional structure develops at larger separations as the temperature was further lowered. This is shown for $T = 0.2$ in Fig. 7. Thus, structure formation in the fluid increases with velocity gradients and with lower temperatures, for the ranges of gradients and temperatures investigated here.

The pair distribution data indicate formation of structure, and this structure is examined in more detail by computing steady state properties of clusters. Appendix A contains the details of how the identity and shape of clusters is determined. The condition that a pair of trimers are members of a cluster is that the distance between the attractive sites is not more that 1.3 units. For the conditions studied in this work, clusters composed of 5 to 15 trimers were globular objects. For larger clusters, the shape is more nearly tubular [35]. The "width" of the clusters was on the order of 2σ to 3σ with the "length", l, of the cluster roughly proportional to the number of trimers, N_C, in the cluster. The dependence of the cluster length on N_c, the number of trimers in the cluster, is illustrated in Fig. 8 for the case of the large velocity gradient at $T = 0.2$ as this state provides the largest range of sizes available in this study. There did not appear to be any strong correlation between the orientation of the tubular structures and the direction of the velocity gradient for the relatively

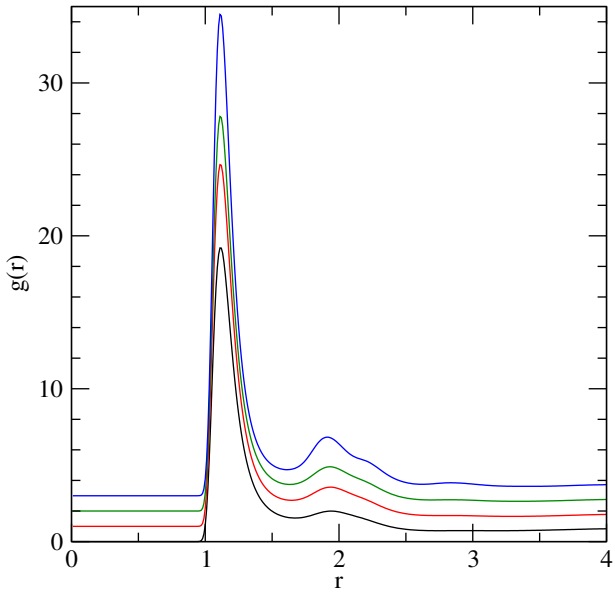

Figure 6: The radial distribution functions, $g(r)$ at $T = 0.30$ for the attractive site pairs are shown for the case of no velocity gradient (black), small velocity gradient (red), medium gradient (green) and large gradient (blue). The functions are vertically offset for clarity.

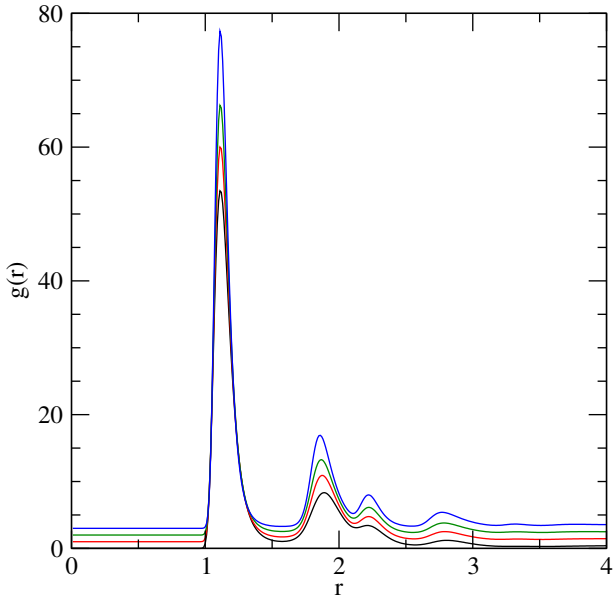

Figure 7: The radial distribution functions, $g(r)$ at $T = 0.20$ for the attractive site pairs are shown for the case of no velocity gradient (black), small velocity gradient (red), medium gradient (green) and large gradient (blue). The functions are vertically offset for clarity.

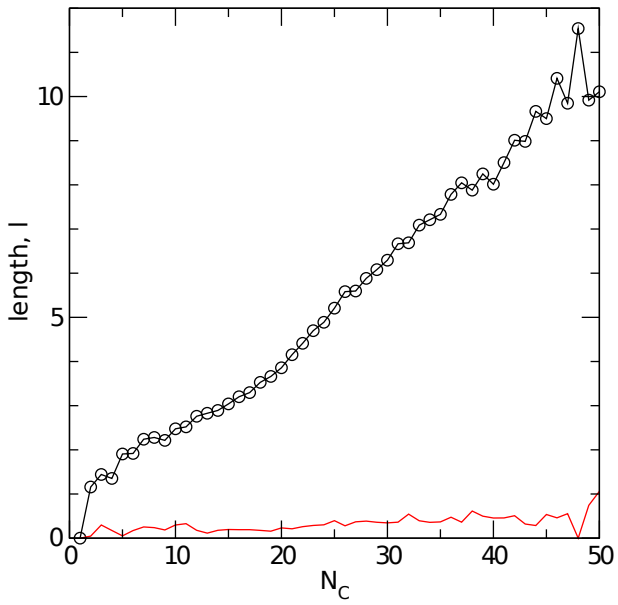

Figure 8: The average length, l, of clusters versus the number of trimers, N_C, in a cluster for $T = 0.20$ with the large velocity gradient is shown in Fig. 4. The symbols are the average length for a given size cluster, and the red line is the standard deviation of the average length.

low particle concentration investigated. For larger numbers of trimers in a cluster, the growth in the average length, l, is approximately a linear function of the number of trimers in the cluster, which implies that the clusters grow approximately linearly in one dimension.

During a simulation, the number of clusters containing N_C trimers was determined and the average number of each size cluster, $P(N_C)$ was obtained. The distribution of the amount of material in clusters containing N_C timers provides an indication of the types of clusters in a system. This is represented by the distribution, $f(N_C)$, which is N_C times the number of clusters containing N_C trimers, $P(N_C)$, divided by the total number of trimers in the system. When $f(N_C)$ is mostly confined to values of N_C less than 5, as shown in the $T = 0.4$ panel Fig. 9, then few, if any, clusters are formed and the fluid is homogeneous. Also, the fraction of "free" trimers not satisfying the cluster criterion was large for $T = 0.4$ and decreases with decreasing temperature.

The presence of a velocity gradient significantly changes the distribution of mass in the clusters. At a given temperature, the mass distribution shifts to larger clusters as the velocity gradient increases. This effect first becomes noticeable at $T = 0.35$. For $T \leq 0.275$, the mass fraction of tubular clusters becomes a significant part of the total mass distribution. In general, the mass fraction, $f(N_C)$, shifts toward larger clusters for a given temperature as the magnitude of the shear increases.

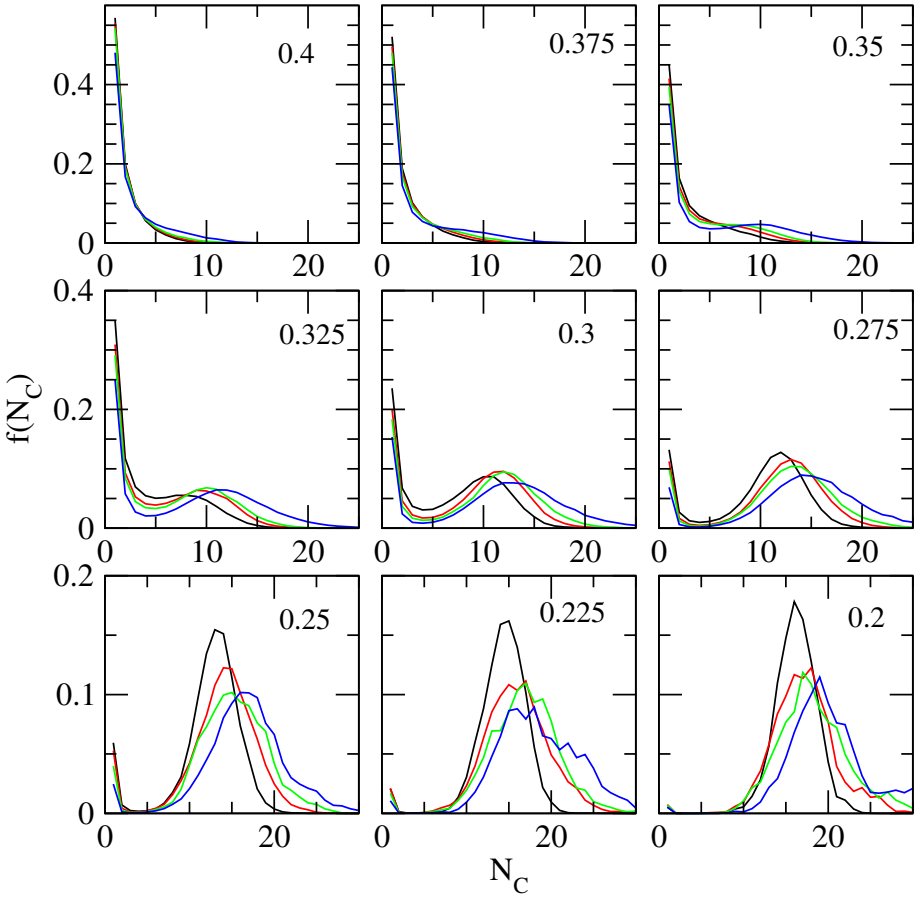

Figure 9: The distribution of the amount of material in clusters is shown for several temperatures, T, as indicated in the upper right corner of each panel. Black (no shear), red (low shear), green (medium shear), blue (high shear). The vertical scales for each row of panels is indicated at the left of the panels.

5. Conclusions

The self-assembly of trimers consisting of one attractive site and two repulsive sites was computationally investigated with nonequilibrium molecular dynamics simulations in the presence of a velocity gradient. Both the magnitude of the shear and the temperature were varied over a range of conditions. Structural quantities were computed to investigate the stability of the resulting globular and tubular self-assembled structures. These quantities include the radial distribution functions, distribution of the amount of material in clusters and the cluster length.

The results of the simulations indicate that the presence of a shear-induced velocity gradient increases the amount of clustering over a wide range of conditions. This may be observed by examining the radial distribution functions, where the second and third peaks become more pronounced with increasing velocity gradient. The amount of clustering in the system also increases as the temperature was lowered, as observed previously [35]. This is reflected by decreases in the internal energy and the heat capacity. A significant indication of clustering is the mass distribution as both functions of temperature and of imposed velocity gradient. An analysis of the clusters indicated that both globular clusters and tubular clusters are formed. The tubular clusters are favored at lower temperatures as indicated in Fig. 9. The feature to emphasize is that tubular clusters containing more than 20 trimers are produced only when a shear is imposed. The presence of a velocity gradient has two consequences. The first is that clusters form at higher temperatures than for the quiescent (*e.g.*, no shear) case. The second is that the formation of tubular clusters is enhanced, in that longer tubular structures are formed at lower temperatures when compared to the case with no velocity gradient. These results on the stability of self-assembled structures under shear may have implications for shear rate sensors and extrusion of self-assembled materials in biomedical and industrial applications [31, 32].

The results in this work are consistent with those observed in a recent simulation study of Janus particles under shear [31, 32]. In particular, cluster sizes were also found to increase with increasing shear rate for the Janus particles. Thus, we show that this effect may also be observed in particles with non-spherical geometries. Note that in Ref. [31], higher shear rates eventually led to a non-monotonic effect where clusters became smaller. Although this shear-induced breakup was not observed in this work, this interesting phenomenon may be observed for trimers in future work at higher shear rates than investigated here [54]. Some hypotheses for the mechanism of increased cluster size with increased shear rate are similar to those postulated for nucleating systems under shear: shear may create defects in ordered structures that serve as nucleation sites which encourages further growth, or promotes coalescence [27, 55, 16, 56]. For all temperatures investigated, the fluid has a slight tendency to thicken as the shear rate increases, which is consistent with the lower shear rate regimes observed in some experiments for micellar systems [52, 53].

6. Acknowledgments

We are grateful to A. Chremos, W. P. Krekelberg and the Fluid Phase Equilibrium reviewers for valuable suggestions. H.W.H. acknowledges support from a National Research Council postdoctoral research associateship at the National Institute of Standards and Technology.

Appendix A. Characterization of clusters in molecular dynamics and Monte Carlo simulations

The task is to determine the members of clusters composed of particles simulated in a molecular dynamics or Monte Carlo study of a fluid state. The following discussion is based on the positions of the attractive sites of the trimers. The positions of the non-attractive sites are ignored. The criterion for membership in a cluster is that a particle is a "near neighbor" of a particle in the cluster with perhaps some other feature such as species taken into account. Here, a pair are neighbors if the distance between the attractive sites is less than 1.3 units [51]. While it is a straightforward task to determine the near neighbors of a given particle, deciding when two well separated particles are in a cluster requires more effort. One approach is described here.

The first step in the process is to construct the neighbor list for each of the N particles in the system. Note that if particle j is a neighbor of particle k, then particle k is also a neighbor of particle j. One also creates an array, *mclus(N)*, that will indicate to which cluster a given particle belongs and an array, *nmember(j,k)*, that contains the list of particles j in cluster k.

Now starting with particle 1, enter the neighbors, j, of 1 in *nmember(j,1)* and assign 1 to *mclus(j)*. Then the neighbors of the neighbors of 1 that are not already in the list are added. This is continued until no further unlisted neighbors are possible. Then this process is repeated with the next particle that is not in a cluster list until all particles have been examined.

The list of clusters is now complete and available for analysis. The feature of interest is the "shape" of the clusters and how the "shape" depends on the presence/absence of shear in the form of a velocity gradient. Our approach is that used by Theodorou and Sutter [57] where the radius of gyration tensor is used to determine the approximate shape of a cluster.

Since the clusters are generated using periodic boundary conditions, it is necessary to first make sure that the cluster is compact. This is done by creating separate lists of the x-, y-, and z-coordinates of the particles in a cluster. These lists are then sorted into increasing order and checked for a difference of more than 1.3 between adjacent entries in the sorted list. If a gap of that magnitude is found, the x-, y-, or z-coordinates of the particles to the right of the gap are shifted to the left by the size of the simulation cell. When this process is finished, the cluster is compact. Clearly, this procedure is appropriate provided the dimensions of the cluster are less than the dimensions of the simulation cell. If this is not the case, the results are system size dependent and will not provide reliable estimates of the cluster size.

The center-of-mass of the compact cluster is determined and the cluster coordinates are rescaled so that the center-of-mass is at the origin of the cluster coordinate system. Next the radius of gyration tensor, $\mathcal{S}$, is constructed where the ij component of $\mathcal{S}$ is

$$\mathcal{S}_{ij} = N_C^{-1} \sum r_{ki} r_{kj} \tag{A.1}$$

where N_C is the number of particles in the cluster and r_{ki} is the i^{th} spatial component particle k in the cluster. The tensor is diagonalized with eigenvalues λ_1^2, λ_2^2 and λ_3^2 and corresponding orthonormal eigenvectors $\mathbf{e_1}$, $\mathbf{e_2}$, and $\mathbf{e_3}$. The largest eigenvalue is λ_3^2 and $\mathbf{e_3}$ specifies the orientation of the major axis of the cluster.

A snapshot of the clusters reveals that the smaller clusters are globular and that the larger ones are roughly cylindrical tubes. The long axis of a cluster is along the unit vector $\mathbf{e}_3$ so the 'length' of a cluster is the distance between the trimers at opposite ends of the cluster that are farthest from the center-of-mass. Specifically the length is taken to be $\mathbf{r}_j \cdot \mathbf{e}_3 - \mathbf{r}_k \cdot \mathbf{e}_3$ where $|\mathbf{r}_j|$ is the largest positive distance from the center-of-mass and $|\mathbf{r}_k|$ is the largest negative distance.

An estimate of the 'width' of a cluster is provided by the moment of inertia of the cluster about the $\mathbf{e}_3$ axis. If one assumes that the density of the cluster about the $\mathbf{e}_3$ axis is uniform with radius R, the moment of inertia, I_3 is $R^2/2$ and the width, W, is then $W = 2\sqrt{2I_3}$. For the clusters discussed here, I_3 is on the order of 0.6 to 0.9, so the width is on the order 2 to 3.

[1] S. Ouk Kim, H. H. Solak, M. P. Stoykovich, N. J. Ferrier, J. J. de Pablo, P. F. Nealey, Epitaxial self-assembly of block copolymers on lithographically defined nanopatterned substrates, Nature 424 (6947) (2003) 411–414. doi:10.1038/nature01775.

[2] M. Grzelczak, J. Vermant, E. M. Furst, L. M. Liz-Marzn, Directed Self-Assembly of Nanoparticles, ACS Nano 4 (7) (2010) 3591–3605. doi:10.1021/nn100869j.

[3] D. E. Angelescu, J. H. Waller, R. A. Register, P. M. Chaikin, Shear-Induced Alignment in Thin Films of Spherical Nanodomains, Adv. Mater. 17 (15) (2005) 1878–1881. doi:10.1002/adma.200401994.

[4] I. Greving, M. Cai, F. Vollrath, H. C. Schniepp, Shear-Induced Self-Assembly of Native Silk Proteins into Fibrils Studied by Atomic Force Microscopy, Biomacromolecules 13 (3) (2012) 676–682. doi:10.1021/bm201509b.

[5] S. Lin, S. Ryu, O. Tokareva, G. Gronau, M. M. Jacobsen, W. Huang, D. J. Rizzo, D. Li, C. Staii, N. M. Pugno, J. Y. Wong, D. L. Kaplan, M. J. Buehler, Predictive modelling-based design and experiments for synthesis and spinning of bioinspired silk fibres, Nat. Commun. 6 (2015) 6892. doi:10.1038/ncomms7892.

[6] L. D. Mayer, M. J. Hope, P. R. Cullis, Vesicles of variable sizes produced by a rapid extrusion procedure, BBA-Biomembranes 858 (1) (1986) 161–168. doi:10.1016/0005-2736(86)90302-0.

[7] N.-J. Cho, L. Y. Hwang, J. J. R. Solandt, C. W. Frank, Comparison of Extruded and Sonicated Vesicles for Planar Bilayer Self-Assembly, Materials 6 (8) (2013) 3294–3308. doi:10.3390/ma6083294.

[8] D. E. Angelescu, J. H. Waller, D. H. Adamson, P. Deshpande, S. Y. Chou, R. A. Register, P. M. Chaikin, Macroscopic Orientation of Block Copolymer Cylinders in Single-Layer Films by Shearing, Adv. Mater. 16 (19) (2004) 1736–1740. doi:10.1002/adma.200400643.

[9] Y.-R. Hong, D. H. Adamson, P. M. Chaikin, R. A. Register, Shear-induced sphere-to-cylinder transition in diblock copolymer thin films, Soft Matter 5 (8) (2009) 1687. doi:10.1039/b820312a.

[10] D. B. Scott, A. J. Waddon, Y. G. Lin, F. E. Karasz, H. H. Winter, Shear-induced orientation transitions in triblock copolymer styrene-butadiene-styrene with cylindrical domain morphology, Macromolecules 25 (16) (1992) 4175–4181. doi:10.1021/ma00042a019.

[11] H. H. Winter, D. B. Scott, W. Gronski, S. Okamoto, T. Hashimoto, Ordering by flow near the disorder-order transition of a triblock copolymer styrene-isoprene-styrene, Macromolecules 26 (26) (1993) 7236–7244. doi:10.1021/ma00078a019.

[12] T. Tepe, M. F. Schulz, J. Zhao, M. Tirrell, F. S. Bates, K. Mortensen, K. Almdal, Variable Shear-Induced Orientation of a Diblock Copolymer Hexagonal Phase, Macromolecules 28 (8) (1995) 3008–3011. doi:10.1021/ma00112a061.

[13] P. D. Butler, L. J. Magid, W. A. Hamilton, J. B. Hayter, B. Hammouda, P. J. Kreke, Kinetics of Alignment and Decay in a Highly Entangled Transient Threadlike Micellar Network Studied by Small-Angle Neutron Scattering, J. Phys. Chem. 100 (2) (1996) 442–445. doi:10.1021/jp9522977.

[14] W.-J. Kim, S.-M. Yang, Flow-Induced Silica Structure during in Situ Gelation of Wormy Micellar Solutions, Langmuir 16 (11) (2000) 4761–4765. doi:10.1021/la9911685.

[15] M. C. Garca-Gutirrez, A. Nogales, D. R. Rueda, C. Domingo, J. V. Garca-Ramos, G. Broza, Z. Roslaniec, K. Schulte, R. J. Davies, T. A. Ezquerra, Templating of crystallization and shear-induced self-assembly of single-wall carbon nanotubes in a polymer-nanocomposite, Polymer 47 (1) (2006) 341–345. doi:10.1016/j.polymer.2005.11.018.

[16] B. J. Ackerson, P. N. Pusey, Shear-Induced Order in Suspensions of Hard Spheres, Phys. Rev. Lett. 61 (8) (1988) 1033–1036. doi:10.1103/PhysRevLett.61.1033.

[17] Y. L. Wu, D. Derks, A. v. Blaaderen, A. Imhof, Melting and crystallization of colloidal hard-sphere suspensions under shear, Proc. Natl. Acad. Sci. USA 106 (26) (2009) 10564–10569. doi:10.1073/pnas.0812519106.

[18] G. H. Fredrickson, Steady shear alignment of block copolymers near the isotropiclamellar transition, J. Rheo. 38 (4) (1994) 1045–1067. doi:10.1122/1.550584.

[19] V. E. Badalassi, H. D. Ceniceros, S. Banerjee, Computation of multiphase systems with phase field models, J. Comput. Phys. 190 (2) (2003) 371–397. doi:10.1016/S0021-9991(03)00280-8.

[20] A. Chremos, K. Margaritis, A. Z. Panagiotopoulos, Ultra thin films of diblock copolymers under shear, Soft Matter 6 (15) (2010) 3588. doi:10.1039/c003198d.

[21] A. Chremos, P. M. Chaikin, R. A. Register, A. Z. Panagiotopoulos, Shear-induced alignment of lamellae in thin films of diblock copolymers, Soft Matter 8 (30) (2012) 7803–7811. doi:10.1039/C2SM25592H.

[22] A. Chremos, P. M. Chaikin, R. A. Register, A. Z. Panagiotopoulos, Sphere-to-Cylinder Transitions in Thin Films of Diblock Copolymers under Shear: The Role of Wetting Layers, Macromolecules 45 (10) (2012) 4406–4415. doi:10.1021/ma300382v.

[23] A. Nikoubashman, R. A. Register, A. Z. Panagiotopoulos, Simulations of shear-induced morphological transitions in block copolymers, Soft Matter 9 (42) (2013) 9960. doi:10.1039/c3sm51759d.

[24] A. Nikoubashman, R. L. Davis, B. T. Michal, P. M. Chaikin, R. A. Register, A. Z. Panagiotopoulos, Thin Films of Homopolymers and Cylinder-Forming Diblock Copolymers under Shear, ACS Nano 8 (8) (2014) 8015–8026. doi:10.1021/nn502068e.

[25] G. Arya, A. Z. Panagiotopoulos, Monte Carlo study of shear-induced alignment of cylindrical micelles in thin films, Phys. Rev. E 70 (3) (2004) 031501. doi:10.1103/PhysRevE.70.031501.

[26] G. Arya, A. Z. Panagiotopoulos, Molecular modeling of shear-induced alignment of cylindrical micelles, Comput. Phys. Commun. 169 (13) (2005) 262–266. doi:10.1016/j.cpc.2005.03.060.

[27] R. J. Allen, C. Valeriani, S. Tnase-Nicola, P. R. t. Wolde, D. Frenkel, Homogeneous nucleation under shear in a two-dimensional Ising model: Cluster growth, coalescence, and breakup, J. Chem. Phys. 129 (13) (2008) 134704. doi:10.1063/1.2981052.

[28] A. Nikoubashman, G. Kahl, C. N. Likos, Cluster Crystals under Shear, Phys. Rev. Lett. 107 (6) (2011) 068302. doi:10.1103/PhysRevLett.107.068302.

[29] S. C. Glotzer, M. J. Solomon, Anisotropy of building blocks and their assembly into complex structures, Nat. Mater. 6 (8) (2007) 557–562. doi:10.1038/nmat1949.

[30] S. Sacanna, D. J. Pine, G.-R. Yi, Engineering shape: the novel geometries of colloidal self-assembly, Soft Matter 9 (34) (2013) 8096–8106. doi:10.1039/C3SM50500F.

[31] E. Bianchi, A. Z. Panagiotopoulos, A. Nikoubashman, Self-assembly of Janus particles under shear, Soft Matter 11 (19) (2015) 3767–3771. doi:10.1039/C5SM00281H.

[32] A. Nikoubashman, E. Bianchi, A. Z. Panagiotopoulos, Correction: Self-assembly of Janus particles under shear, Soft Matter 11 (19) (2015) 3946–3946. doi:10.1039/C5SM90068A.

[33] R. A. DeLaCruz-Araujo, D. J. Beltran-Villegas, R. G. Larson, U. M. Córdova-Figueroa, Rich Janus colloid phase behavior under steady shear 12 (18) (2016) 4071–4081. doi:10.1039/C6SM00183A.

[34] J. R. Wolters, G. Avvisati, F. Hagemans, T. Vissers, D. J. Kraft, M. Dijkstra, W. K. Kegel, Self-assembly of Mickey Mouse shaped colloids into tube-like structures: experiments and simulations, Soft Matter 11 (6) (2015) 1067–1077. doi:10.1039/C4SM02375G.

[35] H. W. Hatch, J. Mittal, V. K. Shen, Computational study of trimer self-assembly and fluid phase behavior, J. Chem. Phys. 142 (16) (2015) 164901. doi:10.1063/1.4918557.

[36] G. Avvisati, M. Dijkstra, Phase separation and self-assembly in a fluid of Mickey Mouse particles, Soft Matter 11 (43) (2015) 8432–8440. doi:10.1039/C5SM02076J.

[37] H. W. Hatch, S.-Y. Yang, J. Mittal, V. K. Shen, Self-assembly of trimer colloids: effect of shape and interaction range, Soft Matter 12 (18) (2016) 4170–4179. doi:10.1039/C6SM00473C.

[38] S. Yadav, S. J. Shire, D. S. Kalonia, Factors affecting the viscosity in high concentration solutions of different monoclonal antibodies, J. Pharm. Sci. 99 (12) (2010) 4812–4829. doi:10.1002/jps.22190.

[39] A. Chaudhri, I. E. Zarraga, S. Yadav, T. W. Patapoff, S. J. Shire, G. A. Voth, The Role of Amino Acid Sequence in the Self-Association of Therapeutic Monoclonal Antibodies: Insights from Coarse-Grained Modeling, J. Chem. Phys. B 117 (5) (2013) 1269–1279. doi:10.1021/jp3108396.

[40] J. D. Weeks, D. Chandler, H. C. Andersen, Role of repulsive forces in determining the equilibrium structure of simple fluids, J. Chem. Phys. 54 (1971) 5237–5247.

[41] J. R. Spaeth, I. G. Kevrekidis, A. Z. Panagiotopoulos, A comparison of implicit- and explicit-solvent simulations of self-assembly in block copolymer and solute systems, J. Chem. Phys. 134 (16) (2011) 164902. doi:10.1063/1.3580293.

[42] A. Jusufi, A. Z. Panagiotopoulos, Explicit- and Implicit-Solvent Simulations of Micellization in Surfactant Solutions, Langmuir 31 (11) (2015) 3283–3292. doi:10.1021/la502227v.

[43] W. Humphrey, A. Dalke, K. Schulten, VMD: Visual molecular dynamics, J. Mol. Graphics 14 (1) (1996) 33–38. doi:10.1016/0263-7855(96)00018-5.

[44] G. J. Martyna, M. L. Klein, M. Tuckerman, Nosé-Hoover chains: The canonical ensemble via continuous dynamics, J. Chem. Phys. 97 (1992) 2635–2643.

[45] N. S. Martys, R. D. Mountain, Velocity Verlet algorithm for dissipative-particle-dynamics-based models of suspensions, Phys. Rev. E 59 (1999) 3733–3736.

[46] D. J. Evans, S. Murad, Singularity free algorithm for molecular dynamics simulation of rigid polyatomics, Mol. Phys. 34 (1977) 327–331.

[47] M. P. Allen, D. J. Tildesley, Computer simulation of liquids, Clarendon Press, 1989, pp 83.

[48] F. Müller-Plathe, Reversing the perturbation in nonequilibrium molecular dynamics: An easy way to calculate the shear viscosity of fluids, Phys. Rev. E 59 (1999) 4894–4898.

[49] T. Müller, M. Al-Samman, F. Müller-Plathe, The influence of thermostats and manostats on reverse nonequilibrium molecular dynamics calculations of fluid viscosities, J. Chem. Phys. 129 (2008) 014102.

[50] R. D. Mountain, System size and control parameter effects in reverse perturbation nonequilibrium molecular dynamics, J. Chem. Phys. 124 (10) (2006) 104109. doi:10.1063/1.2178340.

[51] F. H. Stillinger, Rigorous basis of the Frenkel-Band theory of association equilibrium, J. Chem. Phys. 38 (7) (1963) 1486–1494. doi:10.1063/1.1776907.

[52] J. L. Jones, C. M. Marques, J.-F. Joanny, Shear-Induced Micellization of Diblock Copolymers, Macromolecules 28 (1) (1995) 136–142. doi:10.1021/ma00105a018.

[53] R. Oda, P. Panizza, M. Schmutz, F. Lequeux, Direct Evidence of the Shear-Induced Structure of Wormlike Micelles: Gemini Surfactant 12212, Langmuir 13 (24) (1997) 6407–6412. doi:10.1021/la9621170.

[54] Y. M. Harshe, M. Lattuada, Universal Breakup of Colloidal Clusters in Simple Shear Flow, J. Phys. Chem. B 120 (29) (2016) 7244–7252. doi:10.1021/acs.jpcb.6b03220.

[55] J. J. Cerdà, Shear effects on crystal nucleation in colloidal suspensions, Phys. Rev. E 78 (3) (2008) 031403. doi:10.1103/PhysRevE.78.031403.

[56] M. D. Haw, Direct observation of oscillatory-shear-induced order in colloidal suspensions, Phys. Rev. E 57 (6) (1998) 6859–6864. doi:10.1103/PhysRevE.57.6859.

[57] D. N. Theodorou, W. W. Suter, Shape of unperturbed linear polymers: Polypropylene, Marcromolecules 18 (1985) 1206–1214.